Supplementary Materials

Structure and drug binding of the SARS-CoV-2 envelope protein transmembrane domain in lipid bilayers

Venkata S. Mandala [1], Matthew J. McKay [1], Alexander A. Shcherbakov [1], Aurelio J. Dregni [1], Antonios Kolocouris [2], Mei Hong [1]*

[1] Department of Chemistry, Massachusetts Institute of Technology, Cambridge, Massachusetts, 02139, USA

[2] Department of Pharmaceutical Chemistry, National and Kapodistrian University of Athens, Panepistimioupolis Zografou, Athens 15771, Greece

* Corresponding author: Mei Hong, Professor of Chemistry, email: meihong@mit.edu

This PDF file includes:
Supplementary Tables 1-6 and Supplementary Note 1 containing additional experimental and analysis methods

Supplementary Tables

Supplementary Table 1. ^{13}C and ^{15}N chemical shifts (ppm) of ERGIC-bound ETM at pH 7.5. The ^{13}C and ^{15}N chemical shift uncertainties are ±0.3 ppm and ±0.5 ppm, respectively.

Residue	Cα	Cβ	C'	N	Cγ/γ1	Cγ2	Cδ/δ1	Cδ2	Cε/ Cε1	Cε2/ ζ	Nδ
E8					33.6		181.1				
T9	61.5	67.2		117.5							
G10	44.8		172.7	110.7							
T11	62.5	66.5	173.4	113.5		20.4					
L12	55.7	39.4		121.9	25.0						
I13	62.1	35.3	175.1	119.9	27.1	15.9	10.9				
V14	64.9	29.2	174.7	119.6	21.3	18.8					
N15	53.9	35.4	175.4	117.1	172.2						107.7
S16	60.9	61.0	173.2	116.4							
V17	64.7	29.2	175.4	121.0	21.3	19.4					
L18	55.6	39.0	176.7	118.6	24.7		23.4	18.3			
L19	56.1	39.9	176.0	120.5	24.9						
F20	59.5	37.4	174.5	118.9	136.8		129.3		128.3		
L21	55.5	40.8	176.6	118.8	24.9		23.6	20.2			
A22	53.9	16.5	176.5	123.5							
F23	59.4	37.3	174.3	118.9	137.2		129.3		127.3		
V24	65.4	29.7	175.7	118.3	21.0	18.8					
V25	65.6	29.1	174.8	118.9	21.1	19.5					
F26	60.2	37.0	175.7	119.7	137.0		129.3		128.1		
L27	55.6	39.8	175.9	120.8	25.5		23.8	18.6			
L28	55.5	39.1	176.6	118.4	23.5		23.4	18.8			
V29	64.3	28.7	175.0	119.4	22.2	19.4					
T30	66.9	64.4	173.5	119.2		18.2					
L31	56.5	39.5	176.1	121.7	25.3		25.2	22.3			
A32	53.3	16.5	177.0	123.6							
I33	63.6	36.1	175.0	117.6	28.9	17.1	12.2				
L34	55.9	38.8	176.5	117.0	25.6		25.5	21.5			
T35	60.9	67.4	173.6	102.2		19.8					
A36	51.6	17.6	176.9	123.1							
L37	51.3	36.6	171.0	119.5	24.4		23.3	19.9			
R38	51.8	27.9	178.9	124.4	23.5		39.6			157.3	

Supplementary Table 2. Interhelical ^{1}H-^{1}H distance restraints obtained from the NHHC spectra. The direction of the interhelical contact from the ^{15}N to the ^{13}C is indicated as 'CCW' for counter-clockwise, 'CW' for clockwise, and 'Ambig' for either of the two neighboring helices during structure calculation. "/" in atom designations indicates ambiguous assignment.

Source (^{15}N)	Sink (^{13}C)	Direction	^{1}H-^{1}H SD time (us)	Distance (Å)	Lower Error (Å)	Upper Error (Å)
L12N	T11CA	CCW	500	6.0	3.0	3.0
S16N	L18CA	CCW	500	6.0	3.0	3.0
V14N	S16CB	CW	500	6.0	3.0	3.0
A32N	L31CA	CCW	500	6.0	3.0	3.0
L21N	A22CA	CW	500	6.0	3.0	3.0
L31N	V29CA	CW	500	6.0	3.0	3.0
V29N	T30CB	CCW	1000	6.0	3.0	5.5
S16N	V14CB	CCW	500	6.0	3.0	3.0
V14N	N15CB	CW	500	6.0	3.0	3.0
L28N/V29N	T30CA	Ambig	500	6.0	3.0	3.0
V25N	L21CB	CCW	1000	6.0	3.0	5.5
A22N	F20CB/F23CB	CCW	1000	6.0	3.0	5.5
S16N	T11CG2/L21CD2	CCW	1000	6.0	3.0	5.5
N15N	V14CA/V17CA	CCW	1000	6.0	3.0	5.5
L34N	A36CA	CW	1000	6.0	3.0	5.5
I33N/L34N	T35CA	Ambig	1000	6.0	3.0	5.5
L21N	A22CB	CW	1000	6.0	3.0	5.5
L27N	V25CA	CW	1000	6.0	3.0	5.5
A22N	V17CB	CCW	1000	6.0	3.0	5.5
A32N/A36N	I33CG2	Ambig	1000	6.0	3.0	5.5
L27N	F26CA	CW	1000	6.0	3.0	5.5
L31N	L37CA	CW	1000	6.0	3.0	5.5
T30N/L37N	R38CA	Ambig	1000	6.0	3.0	5.5
L37N	T35CB	Ambig	1000	6.0	3.0	5.5
L21N/F23N	V25CA	CCW	1000	6.0	3.0	5.5
A32N	A36CA/R38CA	Ambig	1000	6.0	3.0	5.5
L34N	I33CG1	Ambig	1000	6.0	3.0	5.5
L31N	V29CB	CW	1000	6.0	3.0	5.5
L27N	V29CB	CW	1000	6.0	3.0	5.5
N15N	S16CA	CW	500	6.0	3.0	3.0
S16N	L21CB	CCW	1000	6.0	3.0	5.5
L19N	V17CA	CCW	500	6.0	3.0	3.0
N15N	L18CA	Ambig	500	6.0	3.0	3.0
S16N	L18CB	CCW	500	6.0	3.0	3.0
V17N	L18CA/L19CA	Ambig	500	6.0	3.0	3.0
L19N	S16CA	CW	500	6.0	3.0	3.0
L31N	I33CG1	CW	500	6.0	3.0	3.0
A32N	T35CG2	Ambig	500	6.0	3.0	3.0
A32N/R38N	I33CG2	Ambig	500	6.0	3.0	3.0

S16N	L18CD2	CCW	500	6.0	3.0	3.0
I33N/L34N	T35CB	Ambig	1000	6.0	3.0	5.5
L31N	A32CB	CW	1000	6.0	3.0	5.5
A32N	A32CB	Ambig	1000	6.0	3.0	5.5
A32N/R38N	A36CA	Ambig	1000	6.0	3.0	5.5
T35N	T35CG2	Ambig	1000	6.0	3.0	5.5
L31N	I33CB	CW	1000	6.0	3.0	5.5
L31N	T30CA	Ambig	1000	6.0	3.0	5.5
A32N	T35CA	Ambig	1000	6.0	3.0	5.5
A32N	T35CB	Ambig	1000	6.0	3.0	5.5
A32N/R38N	L34CG	Ambig	1000	6.0	3.0	5.5
A22N	F20C/F23C	CCW	1000	6.0	3.0	5.5
L28N	T30CG2	Ambig	1000	6.0	3.0	5.5

Supplementary Table 3. Interhelical ^{13}C-^{19}F distance restraints. Positive contacts are ^{13}C sites that show significant REDOR dephasing while negative contacts are sites that do not show significant REDOR dephasing and are thus far from all ^{19}F spins. The direction of the interhelical contact from the ^{19}F spin to ^{13}C is indicated as 'CCW' for counter-clockwise, The experiments that yielded these constraints include broadband ^{13}C-^{19}F REDOR (BB), Cα-selective ^{13}C-^{19}F REDOR (Cα-sel), and water-edited and lipid-edited (Water/lipid) experiments. "/" in atom designations indicates ambiguous assignment.

Dephasing Atom (^{19}F)	Dephased Site (^{13}C)	Direction	Experiment	Distance (Å)	Lower Error (A)	Upper Error (A)	Contact Type
F20HZ	I13CA	Ambig	2D Cα-sel	12.0	4.7	38.0	negative
F20HZ	N15CA	Ambig	2D Cα-sel	9.1	2.0	40.9	negative
F20HZ	S16CA	Ambig	2D Cα-sel	12.0	4.0	38.0	negative
F20HZ	V17CA	Ambig	2D Cα-sel	7.7	2.0	2.0	positive
F26HZ	F23CA	CCW	2D Cα-sel	6.8	2.0	2.0	positive
F20HZ	L21CA	Ambig	2D Cα-sel	6.6	2.0	2.0	positive
F20HZ/F23HZ	A22CA	CW	2D Cα-sel	6.5	2.0	2.0	positive
F26HZ	V24CA	CCW	2D Cα-sel	6.7	2.0	2.0	positive
F23HZ	V25CA	CW	2D Cα-sel	6.7	2.0	2.0	positive
F23HZ	F26CA	CW	2D Cα-sel	6.5	2.6	2.0	positive
F20HZ/F23HZ/ F26HZ	L18CA/L27C A/L28CA	Ambig	2D Cα-sel	7.2	2.0	2.0	positive
F23HZ/F26HZ	V29CA	Ambig	2D Cα-sel	7.7	2.0	2.0	positive
F26HZ	T30CB	CCW	2D Cα-sel	7.1	2.0	2.0	positive
F26HZ	T30CA	Ambig	2D Cα-sel	8.5	2.0	41.5	negative
F26HZ	L31CA	Ambig	2D Cα-sel	7.5	2.0	42.5	negative
F26HZ	A32CA	Ambig	2D Cα-sel	9.5	2.0	40.5	negative
F26HZ	I33CA	Ambig	2D Cα-sel	10.9	2.7	39.1	negative
F26HZ	T35CB	Ambig	2D Cα-sel	12.0	4.8	38.0	negative
F26HZ	T35CA	Ambig	2D Cα-sel	12.0	4.5	38.0	negative
F20HZ	I13CD1	Ambig	1D BB	12.0	2.0	38.0	negative
F20HZ	I13CG2	Ambig	1D BB	8.3	2.0	41.7	negative
F20HZ/F23HZ/ F26HZ	L21CB	Ambig	1D BB	6.1	2.0	2.0	positive
F20HZ	A22CB	CW	1D BB	5.7	2.0	2.0	positive
F26HZ	T30CG2	CCW	1D BB	5.9	2.0	2.0	positive
F26HZ	I33CD1	Ambig	1D BB	12.0	2.0	38.0	negative
F26HZ	A36CA	Ambig	1D Cα-sel	12.0	2.0	38.0	negative
F26HZ	L37CA	Ambig	1D Cα-sel	12.0	2.0	38.0	negative
F26HZ	R38CA	Ambig	1D Cα-sel	12.0	2.0	38.0	negative
F26HZ	R38CB	Ambig	1D BB	12.0	3.4	38.0	negative
F26HZ	R38CZ	Ambig	1D BB	12.0	3.4	38.0	negative
F23HZ	F26CE#/F26 CZ	CW	1D BB	3.3	2.0	2.0	positive
F26HZ	L31CD2	CCW	1D BB	6.4	2.0	2.0	positive
F26HZ	F26HZ	Ambig	Water/lipid	12.0	3.0	38.0	negative
F20HZ	F20HZ	Ambig	Water/lipid	12.0	3.0	38.0	negative
F23HZ	F23HZ	Ambig	Water/lipid	12.0	3.0	38.0	negative

Supplementary Table 4. Agreement of the various pentamer models (Extended Data Figure 7) with experimental ^{13}C-^{19}F data and water-edited 2D NCA spectra.

Model	Unsatisfied ^{13}C-^{19}F Constraints	Unsatisfied Water-Edited Constraints
1: N15***d***, no twist	No intermolecular Phe-Phe contact in this model.	V29 is pore-facing in the model but is poorly hydrated in the water-edited 2D NCA spectra; L31 and T35 are more lipid-facing in the model but are well hydrated in the water-edited spectra.
2: N15***d***, F23***e***→***c***	This model requires the resolved -118 ppm ^{19}F peak to be assigned to F26. Under this condition, the F26HZ – A22 CB cross peak in the 2D C-F spectrum cannot be explained.	V24 is pore-facing and V25 is interfacial in this model, but water-edited spectra show that V25 is better hydrated than V24.
3: N15***e***, F23***f***→***b***	This model requires the resolved -118 ppm ^{19}F peak to be assigned to F26. Under this condition, the F26HZ – A22 CB cross peak in the 2D C-F spectrum cannot be explained; T30 dephasing by F26 in the C-F REDOR data cannot be explained since T30 and F26 are on the same side of the helix so intermolecular dephasing is unlikely.	L19 is lipid-facing in the model but is well hydrated in the water-edited spectra. T35 is interfacial in the model but is well hydrated in the water-edited spectra.
4: N15***a***, F23***b***→***c***	n/a	V24 is pore-facing and V25 is interfacial in the model, but water-edited spectra indicate that V25 is more hydrated than V24; L19 is interfacial in the model, but is well hydrated in the water-edited spectra.
5: N15***a***, F23***b***→***f***	n/a	L19 is interfacial in the model, but is well hydrated in the water-edited spectra.

Supplementary Table 5. XPLOR-NIH parameters for ETM structure calculations.

XPLOR-NIH Potential	Experimental Basis	Restraints per monomer	Round 1 Scale Factor	Round 2 Scale Factor	Best model energy (kcal/mol)
PosDiffPot (ncs)	Single set of chemical shifts	-	100	100	0.83
DistSymmPot	Single set of chemical shifts	-	100	100	0.69
CDIH (dihedral angles)	TALOS-N predictions	56	400	400	1.43
NOE	Intermolecular NHHC contacts	52	0.01-20	0.5-30	186.55
NOE	Intermolecular ^{13}C-^{19}F REDOR	35	0.01-20	0.5-30	
NOE	Intramolecular inter-residue ^{13}C-^{13}C contacts	196	0	0.17-10	
HBDB	α-helical TM for residues 13-19, 23-34	11	1	1	-177.09
TorsionDB	Database favored side-chain rotamers	-	0.0001-0.1	0.01-3	7676.28
BOND	Standard bond lengths	-	1	1	36.36
ANGL	Standard bond angles	-	0.4-1	0.4-1	233.32
IMPR	Standard bond geometry	-	0.1-1	0.1-1	26.70
RepelPot	Non-bonded atomic radii repulsion	-	0.004-4	0.006-6	73.15

Supplementary Table 6. Detailed solid-state NMR experimental parameters for bilayer-bound ETM.

Sample	Experiment	NMR Parameters	Experimental Time
pH 7.5, ERGIC, U-^{13}C, ^{15}N-labeled ETM	2D CC short CORD, high T	B_0 = 21.1 T; $T_{bearing}$ = 293 K; ν_{MAS} = 11.8 kHz, ns = 72, τ_{rd} = 1.7 s, $t_{1,max}$ = 4.4 ms; $t_{1,inc}$ = 25.0 µs; τ_{dwell} = 6.0 µs; τ_{acq} = 10.2 ms; τ_{HC} = 0.5 ms; τ_{CORD} = 20 ms; ν_{1Hacq} = 71 kHz	14 hrs
	2D CC short CORD, low T	B_0 = 21.1 T; $T_{bearing}$ = 263 K; ν_{MAS} = 11.8 kHz, ns = 64, τ_{rd} = 1.7 s, $t_{1,max}$ = 5.0 ms; $t_{1,inc}$ = 25.0 µs; τ_{dwell} = 6.0 µs; τ_{acq} = 10.2 ms; τ_{HC} = 0.5 ms; τ_{CORD} = 20 ms; ν_{1Hacq} = 71 kHz	12 hrs
	2D CC long CORD	B_0 = 21.1 T; $T_{bearing}$ = 293 K; ν_{MAS} = 11.8 kHz, ns = 160, τ_{rd} = 1.6 s , $t_{1,max}$ = 5.0 ms; $t_{1,inc}$ = 22.1 µs; τ_{dwell} = 6.0 µs; τ_{acq} = 12.8 ms; τ_{HC} = 0.5 ms; τ_{CORD} = 250 ms; ν_{1Hacq} = 71 kHz	30 hrs
	2D NCA, high T	B_0 = 21.1 T; $T_{bearing}$ = 293 K; ν_{MAS} = 11.8 kHz, ns = 32, τ_{rd} = 2.0 s, $t_{1,max}$ = 8.9 ms; $t_{1,inc}$ = 127 µs; τ_{dwell} = 5 µs; τ_{acq} = 15.4 ms; τ_{HN} = 0.75 ms; τ_{CN} = 4 ms; $\nu_{15NspecificCP}$ = 30 kHz; $\nu_{13CspecificCP}$ = 18 kHz; ν1HspecificCP = 80 kHz; ν_{1Hacq} = 71 kHz	2.5 hrs
	2D NCA, low T	B_0 = 21.1 T; $T_{bearing}$ = 263 K; ν_{MAS} = 11.8 kHz, ns = 32, τ_{rd} = 2.0 s, $t_{1,max}$ = 8.9 ms; $t_{1,inc}$ = 127 µs; τ_{dwell} = 5 µs; τ_{acq} = 15.4 ms; τ_{HN} = 0.75 ms; τ_{CN} = 4 ms; $\nu_{15NspecificCP}$ = 30 kHz; $\nu_{13CspecificCP}$ = 18 kHz; ν1HspecificCP = 80 kHz; ν_{1Hacq} = 71 kHz	2.5 hrs
	3D NCACX, 28 ms CORD	B_0 = 21.1 T; $T_{bearing}$ = 293 K; ν_{MAS} = 11.8 kHz, ns = 8, τ_{rd} = 2.0 s, $t_{1,max}$ = 5.9 ms; $t_{1,inc}$ = 169.5 µs; $t_{2,max}$ = 4 ms; $t_{2,inc}$ = 100 µs; τ_{dwell} = 5 µs; τ_{acq} = 12.8 ms; τ_{HN} = 0.75 ms; τ_{CN} = 4 ms; $\nu_{15NspecificCP}$ = 30 kHz; $\nu_{13CspecificCP}$ = 18 kHz; τ_{CORD} = 28 ms; ν1HspecificCP = 80 kHz; ν_{1Hacq} = 71 kHz	25 hrs
	3D NCACX, 250 ms CORD	B_0 = 21.1 T; $T_{bearing}$ = 293 K; ν_{MAS} = 11.8 kHz, ns = 24, τ_{rd} = 2.2 s, $t_{1,max}$ = 4.7 ms; $t_{1,inc}$ = 169.5 µs; $t_{2,max}$ = 3.7 ms; $t_{2,inc}$ = 100 µs; τ_{dwell} = 5 µs; τ_{acq} = 12.8 ms; τ_{HN} = 0.75 ms; τ_{CN} = 4 ms; $\nu_{15NspecificCP}$ = 30 kHz; $\nu_{13CspecificCP}$ = 18 kHz; τ_{CORD} = 250 ms; ν1HspecificCP = 80 kHz; ν_{1Hacq} = 71 kHz	69 hrs
	3D NCOCX, 37 ms CORD	B_0 = 21.1 T; $T_{bearing}$ = 293 K; ν_{MAS} = 11.8 kHz, ns = 16, τ_{rd} = 2.0 s, $t_{1,max}$ = 5.9 ms; $t_{1,inc}$ = 169.5 µs; $t_{2,max}$ = 4.4 ms; $t_{2,inc}$ = 169.5 µs; τ_{dwell} = 5 µs; τ_{acq} = 12.8 ms; τ_{HN} = 0.75 ms; τ_{CN} = 4 ms; $\nu_{15NspecificCP}$ = 30 kHz; $\nu_{13CspecificCP}$ = 42 kHz; τ_{CORD} = 37 ms; ν1HspecificCP = 80 kHz; ν_{1Hacq} = 71 kHz	35 hrs
	3D CONCA	B_0 = 21.1 T; T = 293 K; ν_{MAS} = 11.8 kHz, ns = 16, τ_{rd} = 2.0 s, $t_{1,max}$ = 4.1 ms; $t_{1,inc}$ = 169.5 µs; $t_{2,max}$ = 5.8 ms; $t_{2,inc}$ = 169.5 µs; τ_{dwell} =5 µs; τ_{acq} = 12.9 ms; τ_{HC} = 1 ms; τ_{CN} = 4 ms; $\nu_{15NspecificCP}$ = 30 kHz; $\nu_{13CspecificCP}$ = 42 kHz; τ_{NC} = 4 ms; $\nu_{15NspecificCP}$ = 30 kHz; $\nu_{13CspecificCP}$ = 18 kHz; $\nu_{1HspecificCP}$ = 80 kHz; ν_{1Hacq} = 71 kHz	30 hrs
	1D ^{13}C CP	B_0 = 21.1 T; ν_{MAS} = 11.8 kHz, ns = 1024, τ_{rd} = 1.5 s, τ_{dwell} = 6 µs; τ_{acq} = 12.3 ms; τ_{HC} = 0.5 ms; ν_{1Hacq} = 71 kHz	0.4 hrs
	1D ^{15}N CP	B_0 = 21.1 T; ν_{MAS} = 11.8 kHz, ns = 1024, τ_{rd} = 1.6 s, τ_{dwell} = 12 µs; τ_{acq} = 12.3 ms; τ_{HN} = 0.75 ms; ν_{1Hacq} = 71 kHz	0.4 hrs
	1D water-edited ^{13}C CP with 9 ms ^{1}H SD	B_0 = 21.1 T; $T_{bearing}$ = 293 K; ν_{MAS} = 11.8 kHz, ns = 1024, τ_{rd} = 2.0 s, τ_{dwell} = 5 µs; τ_{acq} = 12.8 ms; τ_{1Hexc} = 1.7 ms; τ_{1HSD} = 9 ms; τ_{HC} = 0.5 ms; ν_{1Hacq} = 71 kHz	0.5 hrs
	1D water-edited ^{13}C CP with 100 ms ^{1}H SD	B_0 = 21.1 T; $T_{bearing}$ = 293 K; ν_{MAS} = 11.8 kHz, ns = 1024, τ_{rd} = 2.0 s, τ_{dwell} = 5 µs; τ_{acq} = 12.8 ms; τ_{1Hexc} = 1.7 ms; τ_{1HSD} = 100 ms; τ_{HC} = 0.5 ms; ν_{1Hacq} = 71 kHz	0.5 hrs
	2D water-edited NCA with 9 ms ^{1}H SD	B_0 = 21.1 T; $T_{bearing}$ = 293 K; ν_{MAS} = 11.8 kHz, ns = 640, τ_{rd} = 2.0 s, $t_{1,max}$ = 8.5 ms; $t_{1,inc}$ = 169.5 µs; τ_{dwell} = 5 µs; τ_{acq} = 12.8 ms; τ_{1Hexc} = 1.7 ms; τ_{1HSD} = 9 ms; τ_{HN} = 0.75 ms; τ_{NC} = 4 ms; $\nu_{15NspecificCP}$ = 30 kHz; $\nu_{13CspecificCP}$ = 18 kHz; ν1HspecificCP = 80 kHz; ν_{1Hacq} = 71 kHz	46 hrs

	2D water-edited NCA with 100 ms ^{1}H SD	B_0 = 21.1 T; $T_{bearing}$ = 293 K; ν_{MAS} = 11.8 kHz, ns = 384, τ_{rd} = 2.0 s, $t_{1,max}$ = 8.5 ms; $t_{1,inc}$ = 169.5 µs; τ_{dwell} = 5 µs; τ_{acq} = 12.8 ms; τ_{1Hexc} = 1.7 ms; τ_{1HSD} = 100 ms; τ_{HN} = 0.75 ms; τ_{NC} = 4 ms; $\nu_{15NspecificCP}$ = 30 kHz; $\nu_{13CspecificCP}$ = 18 kHz; $\nu_{1HspecificCP}$ = 80 kHz; ν_{1Hacq} = 71 kHz	23 hrs
	1D lipid-edited ^{13}C CP with 10 ms ^{1}H SD	B_0 = 18.8 T; $T_{bearing}$ = 290 K; ν_{MAS} = 14 kHz, ns = 73728, τ_{rd} = 1.6 s, τ_{dwell} = 6 µs; τ_{acq} = 12.3 ms; τ_{1Hexc} = 2.86 ms; τ_{1HSD} = 10 ms; τ_{HC} = 0.5 ms; ν_{1Hacq} = 71 kHz	35 hrs
	1D lipid-edited ^{13}C CP with 100 ms ^{1}H SD	B_0 = 18.8 T; $T_{bearing}$ = 290 K; ν_{MAS} = 14 kHz, ns = 26624, τ_{rd} = 1.6 s, τ_{dwell} = 6 µs; τ_{acq} = 12.3 ms; τ_{1Hexc} = 2.86 ms; τ_{1HSD} = 100 ms; τ_{HC} = 0.5 ms; ν_{1Hacq} = 71 kHz	12 hrs
pH 7.5, ERGIC, 1 : 1 ^{15}N-labeled : ^{13}C-labeled ETM	NHHC with 0.5 ms ^{1}H SD	B_0 = 18.8 T; $T_{bearing}$ = 290 K; ν_{MAS} = 14 kHz, ns = 1792, τ_{rd} = 1.7 s, $t_{1,max}$ = 5.7 ms; $t_{1,inc}$ = 142.9 µs; τ_{dwell} = 6 µs; τ_{acq} = 10.8 ms; τ_{1HSD} = 0.5 ms; τ_{HN} = 0.75 ms; τ_{NH} = 0.75 ms; τ_{HC} = 0.5 ms; ν_{1Hacq} = 71 kHz	68 hrs
	NHHC with 1 ms ^{1}H SD	B_0 = 18.8 T; $T_{bearing}$ = 290 K; ν_{MAS} = 14 kHz, ns = 2176, τ_{rd} = 1.7 s, $t_{1,max}$ = 5.7 ms; $t_{1,inc}$ = 142.9 µs; τ_{dwell} = 6 µs; τ_{acq} = 10.8 ms; τ_{1HSD} = 1 ms; τ_{HN} = 0.75 ms; τ_{NH} = 0.75 ms; τ_{HC} = 0.5 ms; ν_{1Hacq} = 71 kHz	87 hrs
pH 7.5, ERGIC, 1 : 1, 4-^{19}F-Phe : U-^{13}C, ^{15}N ETM	Broadband 1D ^{13}C-^{19}F REDOR, 5.7 ms (S and S_0 pair)	B_0 = 14.1 T; $T_{bearing}$ = 293 K; ν_{MAS} = 14 kHz, ns = 6144, τ_{rd} = 1.6 s, τ_{dwell} = 8 µs; τ_{acq} = 16.4 ms; τ_{HC} = 0.5 ms; $\tau_{CFREDOR}$=5.7 ms; $\nu_{1HREDOR}$ = 117 kHz; ν_{1Hacq} = 71 kHz	5.5 hrs
	1D Cα-sel ^{13}C-^{19}F REDOR, 10.3 ms (S and S_0 pair)	B_0 = 14.1 T; $T_{bearing}$ = 293 K; ν_{MAS} = 14 kHz, ns = 2048, τ_{rd} = 1.8 s, τ_{dwell} = 8 µs; τ_{acq} = 16.4 ms; $\tau_{13Casel}$ = 286 µs; τ_{HC} = 0.5 ms; $\tau_{CFREDOR}$=10.3 ms; $\nu_{1HREDOR}$ = 117 kHz; ν_{1Hacq} = 71 kHz	2 hrs
	2D ^{13}C-^{13}C resolved ^{13}C-^{19}F REDOR, 10.3 ms (S and S_0 pair)	B_0 = 14.1 T; $T_{bearing}$ = 293 K; ν_{MAS} = 14 kHz, ns = 448, τ_{rd} = 1.8 s, $t_{1,max}$ = 5.4 ms; $t_{1,inc}$ = 64 µs; τ_{dwell} = 8 µs; τ_{acq} = 14.3 ms; $\tau_{13Casel}$ = 286 µs; τ_{HC} = 0.4 ms; $\tau_{CFREDOR}$=10.3 ms; $\nu_{1HREDOR}$ = 117 kHz; ν_{1Hacq} = 71 kHz	76 hrs
	2D ^{13}C-^{19}F double-quantum CP correlation	B_0 = 14.1 T; $T_{bearing}$ = 270 K; ν_{MAS} = 38 kHz, ns = 592, τ_{rd} = 2.0 s, $t_{1,max}$ = 3.7 ms; $t_{1,inc}$ = 33 µs; τ_{dwell} = 3 µs; τ_{acq} = 6.1 ms; τ_{HC} = 1 ms; τ_{CF} = 7 ms; ν_{19F-CP} = 13 kHz; ν_{13C-CP} = 25 kHz; ν_{1H-CP} = 117 kHz; ν_{1Hacq} = 71 kHz	79 hrs
pH 7.5, DMPX	1D ^{13}C CP	B_0 = 18.8 T; ν_{MAS} = 14 kHz, ns = 1024, τ_{rd} = 1.5 s, τ_{dwell} = 6 µs; τ_{acq} = 12.3 ms; τ_{HC} = 0.5 ms; ν_{1Hacq} = 71 kHz	0.4 hrs
	1D ^{13}C DP	B_0 = 18.8 T; ν_{MAS} = 14 kHz, ns = 1024, τ_{rd} = 2.0 s, τ_{dwell} = 6 µs; τ_{acq} = 12.3 ms; ν_{1Hacq} = 71 kHz	0.5 hrs
	1D ^{15}N CP	B_0 = 18.8 T; ν_{MAS} = 14 kHz, ns = 1024, τ_{rd} = 1.6 s, τ_{dwell} = 15 µs; τ_{acq} = 12 ms; τ_{HN} = 0.75 ms; ν_{1Hacq} = 71 kHz	0.4 hrs
	2D CC short CORD, high T	B_0 = 18.8 T; $T_{bearing}$ = 305 K; ν_{MAS} = 14 kHz, ns = 96, τ_{rd} = 1.6 s, $t_{1,max}$ = 6.2 ms; $t_{1,inc}$ = 25.0 µs; τ_{dwell} = 6.0 µs; τ_{acq} = 12.2 ms; τ_{HC} = 0.5 ms; τ_{CORD} = 20 ms; ν_{1Hacq} = 71 kHz	17 hrs
	2D CC short CORD, low T	B_0 = 18.8 T; $T_{bearing}$ = 263 K; ν_{MAS} = 14 kHz, ns = 96, τ_{rd} = 1.6 s, $t_{1,max}$ = 6.2 ms; $t_{1,inc}$ = 25.0 µs; τ_{dwell} = 10.0 µs; τ_{acq} = 12.2 ms; τ_{HC} = 0.5 ms; τ_{CORD} = 20 ms; ν_{1Hacq} = 71 kHz	17 hrs
	2D NC TEDOR	B_0 = 18.8 T; $T_{bearing}$ = 305 K; ν_{MAS} = 14 kHz, ns = 256, τ_{rd} = 2.0 s, $t_{1,max}$ = 10 ms; $t_{1,inc}$ = 142.9 µs; τ_{dwell} = 6 µs; τ_{acq} = 12.3 ms; τ_{HC} = 0.5 ms; τ_{NC} = 1.43 ms; ν_{1Hacq} = 71 kHz	20 hrs
	2D NC TEDOR	B_0 = 18.8 T; $T_{bearing}$ = 263 K; ν_{MAS} = 14 kHz, ns = 256, τ_{rd} = 2.0 s, $t_{1,max}$ = 10 ms; $t_{1,inc}$ = 142.9 µs; τ_{dwell} = 6 µs; τ_{acq} = 12.3 ms; τ_{HC} = 0.5 ms; τ_{NC} = 1.43 ms; ν_{1Hacq} = 71 kHz	20 hrs

pH 7.5, DMPX, HMA : ETM (4 : 1)	2D CC short CORD	B_0 = 18.8 T; $T_{bearing}$ = 305 K; ν_{MAS} = 14 kHz, ns = 96, τ_{rd} = 1.6 s, $t_{1,max}$ = 6.2 ms; $t_{1,inc}$ = 25.0 µs; τ_{dwell} = 6.0 µs; τ_{acq} = 12.2 ms; τ_{HC} = 0.5 ms; τ_{CORD} = 20 ms; ν_{1Hacq} = 71 kHz	17 hrs
	2D NC TEDOR	B_0 = 18.8 T; $T_{bearing}$ = 305 K; ν_{MAS} = 14 kHz, ns = 224, τ_{rd} = 2.0 s, $t_{1,max}$ = 10 ms; $t_{1,inc}$ = 142.9 µs; τ_{dwell} = 6 µs; τ_{acq} = 12.3 ms; τ_{HC} = 0.5 ms; τ_{NC} = 1.43 ms; ν_{1Hacq} = 71 kHz	17 hrs
pH 7.5 DMPX AMT : ETM (8 : 1)	1D ^{19}F DP	B_0 = 14.1 T; $T_{bearing}$ = 270 K; ν_{MAS} = 14 kHz, ns = 10240, τ_{rd} = 1.5 s, τ_{dwell} = 6 µs; τ_{acq} = 6.1 ms; ν_{1Hacq} = 71 kHz	4.3 hrs
	1D broadband ^{13}C-^{19}F REDOR, 9.1 ms (S and S_0 pair)	B_0 = 14.1 T; $T_{bearing}$ = 270 K; ν_{MAS} = 14 kHz, ns = 5120, τ_{rd} = 1.8 s, τ_{dwell} = 8 µs; τ_{acq} = 6.1 ms; τ_{HC} = 0.5 ms; $\tau_{CFREDOR}$=9.1 ms; $\nu_{1HREDOR}$ = 117 kHz; ν_{1Hacq} = 71 kHz	5.2 hrs
	1D broadband ^{13}C-^{19}F REDOR, 11.4 ms (S and S_0 pair)	B_0 = 14.1 T; $T_{bearing}$ = 270 K; ν_{MAS} = 14 kHz, ns = 5120, τ_{rd} = 1.8 s, τ_{dwell} = 8 µs; τ_{acq} = 6.1 ms; τ_{HC} = 0.5 ms; $\tau_{CFREDOR}$=11.4 ms; $\nu_{1HREDOR}$ = 117 kHz; ν_{1Hacq} = 71 kHz	5.2 hrs
	1D Cα-selective ^{13}C-^{19}F REDOR, 10.0 ms (S and S_0 pair)	B_0 = 14.1 T; $T_{bearing}$ = 270 K; ν_{MAS} = 14 kHz, ns = 5120, τ_{rd} = 1.8 s, τ_{dwell} = 8 µs; τ_{acq} = 6.1 ms; $\tau_{13C\alpha sel}$ = 286 µs; τ_{HC} = 0.5 ms; $\tau_{CFREDOR}$=10.0 ms; $\nu_{1HREDOR}$ = 117 kHz; ν_{1Hacq} = 71 kHz	5.2 hrs
	1D Cα-selective ^{13}C-^{19}F REDOR, 14.3 ms (S and S_0 pair)	B_0 = 14.1 T; $T_{bearing}$ = 270 K; ν_{MAS} = 14 kHz, ns = 5120, τ_{rd} = 1.8 s, τ_{dwell} = 8 µs; τ_{acq} = 6.1 ms; $\tau_{13C\alpha sel}$ = 286 µs; τ_{HC} = 0.5 ms; $\tau_{CFREDOR}$=14.3 ms; $\nu_{1HREDOR}$ = 117 kHz; ν_{1Hacq} = 71 kHz	5.2 hrs
	2D CC short CORD	B_0 = 18.8 T; $T_{bearing}$ = 263 K; ν_{MAS} = 14 kHz, ns = 96, τ_{rd} = 1.6 s, $t_{1,max}$ = 6.2 ms; $t_{1,inc}$ = 25.0 µs; τ_{dwell} = 6.0 µs; τ_{acq} = 12.2 ms; τ_{HC} = 0.5 ms; τ_{CORD} = 20 ms; ν_{1Hacq} = 71 kHz	17 hrs
	2D NC TEDOR	B_0 = 18.8 T; $T_{bearing}$ = 305 K; ν_{MAS} = 14 kHz, ns = 256, τ_{rd} = 2.0 s, $t_{1,max}$ = 10 ms; $t_{1,inc}$ = 142.9 µs; τ_{dwell} = 6 µs; τ_{acq} = 12.3 ms; τ_{HC} = 0.5 ms; τ_{NC} = 1.43 ms; ν_{1Hacq} = 71 kHz	20 hrs
pH 5.0, DMPX No Salt	2D CC short CORD	B_0 = 18.8 T; $T_{bearing}$ = 305 K; ν_{MAS} = 14 kHz, ns = 96, τ_{rd} = 1.6 s, $t_{1,max}$ = 6.2 ms; $t_{1,inc}$ = 25.0 µs; τ_{dwell} = 10.0 µs; τ_{acq} = 12.2 ms; τ_{HC} = 0.5 ms; τ_{CORD} = 20 ms; ν_{1Hacq} = 71 kHz	17 hrs
pH 5.0, DMPX 5 mM $CaCl_2$	2D CC short CORD	B_0 = 18.8 T; $T_{bearing}$ = 305 K; ν_{MAS} = 14 kHz, ns = 96, τ_{rd} = 1.6 s, $t_{1,max}$ = 6.2 ms; $t_{1,inc}$ = 25.0 µs; τ_{dwell} = 10.0 µs; τ_{acq} = 12.2 ms; τ_{HC} = 0.5 ms; τ_{CORD} = 20 ms; ν_{1Hacq} = 71 kHz	17 hrs
	2D NC TEDOR	B_0 = 18.8 T; $T_{bearing}$ = 305 K; ν_{MAS} = 14 kHz, ns = 224, τ_{rd} = 2.0 s, $t_{1,max}$ = 10 ms; $t_{1,inc}$ = 142.9 µs; τ_{dwell} = 6 µs; τ_{acq} = 12.3 ms; τ_{HC} = 0.5 ms; τ_{NC} = 1.43 ms; ν_{1Hacq} = 71 kHz	17 hrs

Definitions of symbols: B_0 = magnetic field; $T_{bearing}$ = thermocouple-reported bearing gas temperature; ν_{MAS} = MAS frequency; ns = number of scans per free induction decay; τ_{rd} = recycle delay; $t_{1,max}$ = maximum t_1 evolution time; $t_{1,inc}$ = t_1 increment; $t_{2,max}$ = maximum t_2 evolution time; $t_{2,inc}$ = t_2 increment; τ_{dwell} = dwell-time in the direct dimension; τ_{acq} = maximum acquisition time in the direct dimension; τ_{HC} = ^{1}H-^{13}C cross polarization contact time; τ_{CORD} = ^{13}C-^{13}C mixing time using CORD; ν_{1Hacq} = ^{1}H rf field strength for decoupling during acquisition; τ_{NC} = total ^{15}N-^{13}C TEDOR recoupling time; τ_{HN} = ^{1}H-^{15}N cross polarization contact time; τ_{1Hexc} = ^{1}H 90° pulse length for selective excitation of water; τ_{1HSD} = ^{1}H-^{1}H spin diffusion mixing time; $\tau_{13C\alpha sel}$ = 180° pulse length for selective inversion of Cα resonances; $\tau_{CFREDOR}$ = total ^{13}C-^{19}F REDOR recoupling time; $\nu_{1HREDOR}$ = ^{1}H rf field strength for decoupling during ^{13}C-^{19}F REDOR.

Supplementary Note 1

Synthesis of F-Amt

The synthetic protocol (Scheme S1) used for preparation of F-Amt was adapted from that described by Jasys and coworkers [44]. Thus, the reaction between 1-adamantanecarboxylic acid and $KMnO_4$ afforded 3-hydroxyadamantanecarboxylic acid which was transformed through its tetrabutylammonium salt to the corresponding methyl ester. The fluorination of the hydroxyester was accomplished through treatment with diethylaminosulfur trifluoride (DAST) at -50 °C. The 3-fluoroadamantane-1-amine acetate (F-Amt acetate) was obtained by treatment of 3-fluoroadamantanecarboxylic acid with diphenylphosphorylazide (DPPA) and subsequent hydrogenolysis of the resultant benzyl carbamate.

Scheme S1

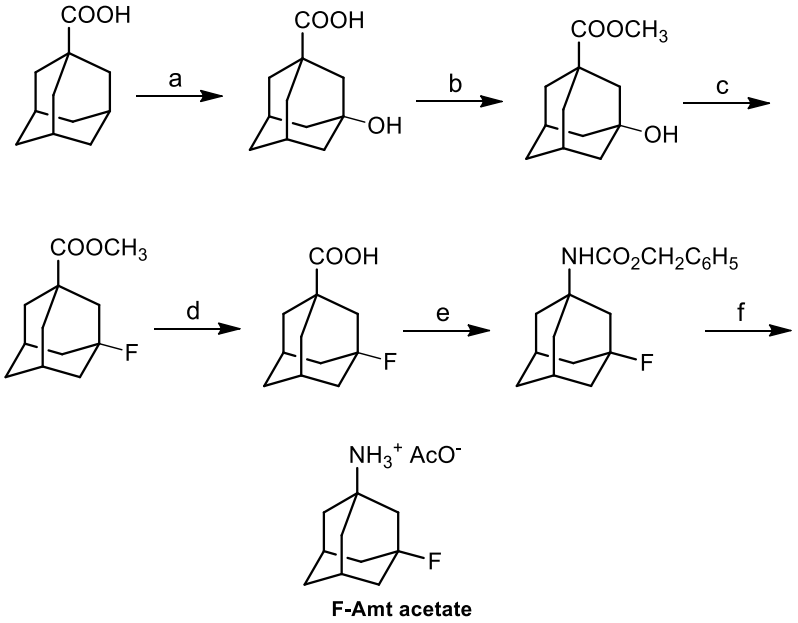

F-Amt acetate

Reagents and Conditions: (a) $KMnO_4$, KOH, 50 °C; (b) $TBAHSO_4$, $NaHCO_3$, CH_3I, acetone, 48 h, r.t.; (c) DAST, CH_2Cl_2, 3 h, -50 °C → 60 °C; (d) NaOH, MeOH, THF, H_2O, 24 h, r.t.; (e) DPPA, TEA, BnOH, benzene, 70 °C; (f) H_2, 10 % Pd/C, AcOH.

3-fluoroadamantane-1-amine acetate (F-Amt acetate): ^{1}H-NMR (phosphate buffer, pH 7, 10 % D_2O, 500 MHz) δ (ppm) 1.60-1.69 (m, 2H, 6-H), 1.87 (s, 4H, 4,10-H), 1.89-1.98 (m, 7H, 8,9-H, CH_3COO^-), 2.09 (br d, 2H, 2-H), 2.48 (br s, 2H, 5,7-H); LC-MS (m/z) 170.3 ($FC_{10}H_{14}NH_3^+$). *Base:* mp 210 °C (EtOH-ether); ^{1}H-NMR ($CDCl_3$, 400 MHz) δ (ppm) 1.41 (br s, 2H, 6-H), 1.49 (br s, 2H, NH_2), 1.51 (br s, 4H, 4,10-H), 1.74 (br d, 2H, J = 5.8 Hz, 2-H), 1.79 (br m, 4H, 8,9-H), 2.31 (br s, 2H, 5,7-H); ^{13}C-NMR ($CDCl_3$, 50 MHz) δ (ppm) 31.33, 31.55 (5,7-C), 34.67 (6-C), 41.44, 41.77 (4,10-C), 44.74 (8,9-C), 51.14, 51.47 (2-C, 3-C), 93.29 (d, $J_{C\text{-}F}$ = 183.8 Hz, 1-C). Anal. Acetate ($C_{12}H_{20}NO_2F$) (EtOH-Et_2O). Calc. C: 62.86 H: 8.79. Found. C: 62.56 H: 8.99.

Additional membrane sample preparation protocols

Chemical shift assignment and interhelical distance measurements were conducted on ETM bound to an ERGIC-mimetic membrane [42,43] containing 1-palmitoyl-2-oleoyl-glycero-3-

phosphocholine (POPC), 1-palmitoyl-2-oleoyl-sn-glycero-3-phosphoethanolamine (POPE), bovine phosphatidylinositol (PI), 1-palmitoyl-2-oleoyl-sn-glycero-3-phospho-L-serine (POPS), and cholesterol (Chol). The POPC : POPE : PI : POPS : Chol molar ratios were 45 : 20 : 13 : 7 : 15. All lipids were purchased from Avanti Polar Lipids. The membrane has a protein : lipid molar ratio (P : L) of 1 : 20, and 2–4 mg ^{13}C, ^{15}N-labeled protein was used for most 2D and 3D correlation experiments. The intermolecular NHHC spectra were measured using a sample containing 4 mg each of ^{13}C-labeled ETM and ^{15}N-labeled ETM. This mixture was reconstituted into the ERGIC membrane at a P : L of 1 : 10 to increase the experimental sensitivity. ^{13}C-^{19}F REDOR experiments were conducted on 3.7 mg total of 1 : 1 mixed ^{13}C-labeled and fluorinated ETM bound to the ERGIC membrane at P : L = 1 : 10.

To reconstitute ETM into lipid bilayers, we dissolved 2 mg protein in 1 mL trifluoroethanol (TFE) and mixed with appropriate amounts of lipids in 400 µL chloroform. For the HMA-bound sample, HMA was dissolved in TFE (1 mg/100 µL) and added to the protein-lipid mixture. The organic solvents were removed under a gentle stream of nitrogen gas, and the film was dried under vacuum at room temperature overnight. The proteoliposome film was resuspended in 3 mL of pH 7.5 sample buffer by vortexing and sonicating 2-3 times for 5 min until the suspension was homogenous. This was followed by 7 freeze-thaw cycles between a 42°C water bath and liquid nitrogen. The proteoliposomes were then pelleted using ultracentrifugation for 3 hours at 164,000x g and 4°C. The pellet was dried in a desiccator or under a gentle stream of nitrogen gas to a final hydration level of ~40% by mass and then packed into an appropriate MAS rotor using a benchtop centrifuge.

Drug binding to ETM was assessed in a “DMPX” membrane consisting of 1,2-dimyristoyl-sn-glycero-3-phosphocholine (DMPC) : 1,2-dimyristoyl-sn-glycero-3-phospho-(1'-rac-glycerol) (DMPG) at a 80% : 20% molar ratio. The mixture was chosen to maintain the same 20% anionic lipid fraction as the ERGIC membrane. A drug-free sample contained 2 mg of U-^{13}C, ^{15}N-labeled ETM bound to the membrane at a P : L of 1 : 20. The sample containing 5-(N,N-hexamethylene)-amiloride (HMA) was prepared using a protein : drug (P : D) molar ratio of 1 : 1, with HMA (0.2 mg) added during organic solution mixing. The same P : L of 1:20 as the apo sample was used. After initial spectra showed only small CSPs, we titrated an additional 0.6 mg of HMA in 6 µl dimethyl sulfoxide (DMSO) into the proteoliposome, giving a P : D of 1 : 4. The solubility of HMA in aqueous solutions was very low (< 0.1 mg/ml), necessitating the use of DMSO. 3-^{19}F-amantadine (AMT) was titrated into the proteoliposome stepwise, from an initial P : D molar ratio of 1 : 1 to a final P : D of 1 : 8. The protein/lipid molar ratio of the sample is 1 : 15. The fluorinated AMT has high solubility in water, thus can be mixed with the membrane directly. For the ^{13}C-^{19}F REDOR experiments, the sample was packed in a 1.9 mm MAS rotor, while chemical shift measurements were conducted in a 3.2 mm MAS rotor on the 800 MHz spectrometer.

Chemical shift changes under acidic pH and with added calcium were assessed in the same “DMPX” membrane. The sample with 5 mM $CaCl_2$ at pH 5 contained 2 mg of U-^{13}C, ^{15}N-labeled ETM bound to the membrane at a P : L of 1 : 20, while the sample without calcium contained 2 mg of U-^{13}C-labeled ETM bound to the membrane at a P : L of 1 : 20.

Simulation of ^{13}C-^{19}F REDOR curves

^{13}C-^{19}F REDOR data were simulated using the SIMPSON software [55]. The simulations accounted for finite ^{19}F and ^{13}C 180° pulse lengths and ^{19}F pulse imperfections by co-adding REDOR curves for ^{19}F flip angles of 180° to 145° using a normal distribution centered at 180° with a standard deviation of 15° [50]. The simulations also included ^{19}F chemical shift anisotropy (CSA), which was measured from the ^{19}F CSA sideband patterns in spectra measured at 293 K under 14 kHz MAS. The sideband intensities were fit using the Solids Lineshape Analysis module in Topspin. The

best-fit CSA was δ_{CSA} = 55±2 ppm and η = 0.6±0.1 for the ^{19}F peak at δ_{iso} = -113.5 ppm and δ_{CSA} = 53±2 ppm and η = 0.5±0.1 for the ^{19}F peak at δ_{iso} = -117.5 ppm. These CSAs indicate that all three 4-^{19}F-Phe residues are immobilized.

REDOR distance analysis required two other considerations. First, the 1 : 1 ^{13}C and ^{19}F mixed peptides means that only 50% of all ^{13}C-labeled helices have an adjacent ^{19}F-labeled helix. Thus, the lowest possible REDOR S/S_0 value is 0.5. Second, while most ^{13}C-^{19}F REDOR restraints came from 2D ^{13}C-^{13}C resolved peaks, dephasing to sidechain carbons were obtained from 1D ^{13}C spectra with resonance overlap. These overlapped peaks will not experience complete dipolar dephasing if some of the carbons contributing to an overlapped signal are far from a fluorine. We first identified the residues experiencing dephasing by ^{19}F from the 2D ^{13}C-^{13}C correlation spectra. These peaks then guided the assignment of the 1D ^{13}C-^{19}F spectra. For example, both A22 and A32 Cβ resonate at 16.6 ppm, but only A22 Cα is dephased in the 2D ^{13}C-^{13}C spectrum (**Fig. 2b**). Thus, we assigned the 16.6 ppm dephased signal in the 1D ^{13}C-^{19}F REDOR spectra to A22 Cβ. Making the reasonable assumption that each Ala Cβ contributes equal intensity, we account for this overlap factor by correcting the experimental dephasing $(S/S_0)_{exp}$ values according to:

$$\left(S/S_0\right)_{adj} = 1 - \left[2 \times \left(1 - \left(S/S_0\right)_{exp}\right) \times f\right] \qquad (2)$$

where *f* is the fraction of an overlapped ^{13}C peak that is dephased by ^{19}F. For example, for the 2-fold overlapped 16.6-ppm Ala Cβ peak with *f* = 2, the lowest possible $(S/S_0)_{exp}$ value is ~0.75, which gives a minimal $(S/S_0)_{adj}$ of ~0.0.

The random uncertainty $\sigma(S/S_0)_{exp}$ of the measured $(S/S_0)_{exp}$ values were propagated from the signal-to-noise ratios (SNRs) of the REDOR S_0 and S spectra. The upper and lower limits for the $(S/S_0)_{adj}$ values were obtained by adding or subtracting the $\sigma(S/S_0)_{exp}$ to the $(S/S_0)_{exp}$ values before using equation (2), respectively. Best-fit distances were obtained as the distance with the lowest χ^2 value between the $(S/S_0)_{adj}$ values and simulated S/S_0 intensities. Upper and lower distance limits were specified using the upper and lower limits for the $(S/S_0)_{adj}$ values calculated as described above. For an upper limit of $(S/S_0)_{adj}$ >0.95 indicating a negative contact (i.e. dephasing was not significant), an upper limit of 50 Å was used. The final lower and upper distance limits for structure calculation were set by multiplying the uncertainty obtained in this manner by 2 times or by choosing distances that are 2.0 Å from the best-fit value, whichever was larger, to loosen the constraints.

Docking of HMA to ETM structure

The coordinate file for HMA was generated from bond connectivity using the Chem3D module of ChemDraw Professional 18.1. Ligand geometry was optimized within Chem3D using the MM2 energy minimization module. Docking was performed using the HADDOCK 2.4 webserver using the ensemble of the ten lowest-energy protein structures calculated in XPLOR-NIH. The docking was constrained only with an active list. Active residues were defined as the N-terminal residues with significant CSPs (**Fig. 4c),** including T9, G10, T11, I13, and S16. Several docking runs were conducted using constraints to this list of residues on all helices, one of the five helices, and different combinations of two of the five helices. Docking calculations were performed using default settings in the HADDOCK 2.4 webserver interface, except that the solvent for the final structural refinement were varied as DMSO and water. The N- and C-termini were set as uncharged as the structural model does not include the full protein sequence. Passive residues were automatically defined around the active residues with a 6.5 Å surface radius cutoff. Non-polar hydrogens were removed from the calculation, and 2 partitions for random exclusion of Ambiguous Interaction Restraints ('AIRs') were used (50% of AIRs were randomly excluded in

the calculation). The docking used 1000 structures for rigid-body docking with 5 trials of rigid-body minimization. Semi-flexible refinement was done with 200 structures selected from the rigid-body minimization stage. Final refinement with explicit solvent (DMSO or water) were performed on all 200 structures from semi-flexible refinement. Output structures were aligned and analyzed in Pymol 2.3.5.

In docking with DMSO as a refinement solvent, 200 refined structures were grouped into 5 clusters, with 154 structures belonging to the lowest energy cluster 1. The four best structures of this cluster had an average HADDOCK score of -29.8 +/- 2.1, and a Z-score of -1.7. Similar results were obtained with docking with water as a refinement solvent, the 200 refined structures were grouped into three clusters, where cluster 1 contained 170 structures. The four best structures this cluster had a HADDOCK score of -29.3 +/- 1.9, with a Z-score of -1.4.

The majority of docked structures converged to a state where HMA partitioned to the N-terminal entry cavity of the channel, but the HMA orientation is variable. Visual inspection showed three distinct orientations: 1) HMA tilted and diving into the pore with the hexamethylene ring facing up (**Extended Data Fig. 9a**), 2) HMA tilted and diving into the pore with the ring facing down (**Extended Data Fig. 9b**), 3) HMA laying horizontally across the top of the channel, with the guanidinium intercalated between two helices (**Extended Data Fig. 9c**). Among the 32 lowest energy structures in the DMSO and water docking results, 13/32 structures belonged to the first mode (ring up), 6/32 to the second mode (ring down), and 13/32 to the third mode (horizontal). All these modes indicate a pore-occlusion mechanism, similar to the amantadine inhibition mechanism of the influenza AM2 proton channel [9].

Given the hydrophobic nature of HMA, another possible binding mode would be drug binding from the lipid side to the exterior of the helical bundle. This mode could explain the chemical shift perturbation of the lipid-facing S16, but the mechanism of inhibition would be indirect allosteric narrowing of the pore, and would require multiple drug molecules to bind each pentamer to preserve the symmetry, as only a single set of peaks are observed in the drug-bound protein spectra. Thus we consider this mechanism less likely than direct occlusion of the pore. The lipid-binding mode was only observed in docking runs with only one or two helices containing the active residues.